CHEMISTRY
A EUROPEAN JOURNAL

DOI: 10.1002/chem.200701613

Nonpolar Dihydrogen Bonds—On a Gliding Scale from Weak Dihydrogen Interaction to Covalent H–H in Symmetric Radical Cations $[H_nE\text{-}H\text{-}H\text{-}EH_n]^+$

Andreas Krapp,[b] Gernot Frenking,*[b] and Einar Uggerud*[a]

Dedicated to Professor Boche on the occasion of his 70th birthday

Abstract: The electronic structures and bonding patterns for a new class of radical cations, $[H_nE\text{-}H\text{-}H\text{-}EH_n]^+$ (EH_n = element hydride, E = element of Groups 15–18), have been investigated by applying quantum-chemical methods. All structures investigated give rise to symmetric potential energy minimum structures. We envisage clear periodic trends. The H–H bond length is shorter for elements toward the bottom of the periodic table of elements, and a short H–H bond corresponds to accumulation of electron density in the central H–H region. All $[H_nE\text{-}H\text{-}H\text{-}EH_n]^+$ of Groups 15–17 are thermodynamically unstable towards loss of either H_2 or H. The barriers for these dissociations are rather low. The Group 18 congeners, except E = Xe, appear to be global minima of the respective potential energy surfaces. The findings are discussed in terms of H_2 bond activation, and a general mechanistic scheme for the standard reduction process $2H^+ + 2e^- \rightarrow H_2$ is given. Finally, it is proposed that some of the symmetric radical cations are likely to be observed in mass spectrometric or matrix isolation experiments.

Keywords: gas phase ion chemistry · H–H bond activation · mass spectrometry · matrix isolation · quantum-chemical methods

Introduction

One of the major challenges to mankind in the 21st century is the realization of renewable and sustainable energy sources. The use of dihydrogen, H_2, in particular for automotive purposes, is one of the most promising approaches. To facilitate this it is mandatory to develop new strategies for safe storage and to find efficient solutions to H_2 combustion, including fuel cell technology. From a chemical point of view, success in this field will depend on an accurate and fundamental understanding of all aspects of the properties and reactivity of H_2 itself, in particular how the molecule responds to different atomic and molecular environments. In this respect, identifying new structural motifs that either can be directly embedded in storage or combustion devices, or inspire development of new materials, will be of interest. Herein we present a new type of structural motif, E-H-H-E, in which dihydrogen bridges two main group elements, forming a central symmetrical arrangement, which represents a wide range of H–H bonding depending on the element in question. Before describing our findings in more detail, it will be useful to review briefly what is already known about the various types of binding between two hydrogen atoms, ranging from the weak polar dihydrogen bond to the strong nonpolar covalent bond found in the H_2 molecule.

The concept of the dipolar dihydrogen bond was introduced in 1995,[1] but the existence of a weak interaction between oppositely charged hydrogen atoms in the form of $H(\delta^+)\cdots H(\delta^-)$ had been indicated long before that. Already in 1934, Zakariassen and Mooney[2] inferred a close contact between the two types of hydrogen in crystals of ammonium hypophosphite. In a 1964 paper Burg[3] reported shifts in infrared (IR) absorption lines of amine borides, an effect that does not show up in the spectra of the analogous phosphine borides. The full significance of this observation as being due to an intermolecular (B)–H···H–(N) interaction was noted in a 1968 paper by Brown et al.[4] applying somewhat more informative IR techniques. An early example of an intramolecular $H(\delta^+)\cdots H(\delta^-)$ interaction was reported in a paper from 1990 by Stevens et al.[5] on crystals of *cis*-$[IrH(OH)(PMe_3)_4]PF_6$. Close H···H contacts (1.75–2.20 Å) have been inferred from studies of various inorganic hy-

[a] Prof. Dr. E. Uggerud
Senter for teoretisk og beregningsbasert kjemi (CTCC)
Kjemisk institutt, Universitetet i Oslo
Postboks 1033 Blindern, 0315 Oslo (Norway)
Fax: (+47) 22-85-5441
E-mail: einar.uggerud@kjemi.uio.no

[b] Dr. A. Krapp, Prof. Dr. G. Frenking
Fachbereich Chemie, Phillipps-Universität Marburg
Hans-Meerwein-Strasse, 35032 Marburg (Germany)
E-mail: frenking@chemie.uni-marburg.de

drides, and an account that sums up the most important results published up to 1996 can be found in reference [6]. A recent (2001) review summarizes most of the literature related to this thought-provoking concept.[7]

Quantum-chemical calculations support the notion of a dipolar dihydrogen bond, as described above. Grabowski[8] studied complexes of the type $H_nA{-}H\cdots H{-}F$. The interaction becomes stronger the more electropositive is the element A. However, a detailed quantum chemical analysis of complexes of the type Li–H···H–X and Na–H···H–X (X = halide) by Hugas et al.[9] revealed that when the H–X bond becomes sufficiently polar, the dihydrogen bonded structure no longer corresponds to a potential minimum, but collapses spontaneously into LiX + H_2 and NaX + H_2, respectively, precluding stable molecules of these types with H···H contacts shorter than 1.6 Å. In addition to having an electrostatic component, analysis of the interaction energy components and one-electron density transfer of dipolar dihydrogen bonds has shown that non-electrostatic effects are responsible for bond elongation and shortening.[10]

Following the discoveries of H_3O^- and NH_4^-, in 1986 Cremer and Kraka[11] studied interactions between the hydride ion and some simple molecules. Their MP2/6–31++G(d,p) calculations suggested the existence of two forms of these complexes, $H_nA{-}H\cdots H^-$ and $H_nA^-\cdots H_2$, separated by a barrier for the interconnecting proton transfer. The shortest H···H distance reported was for $F{-}H\cdots H^-$ (1.15 Å). It is also known that even electrically neutral radical sites may act as hydrogen bond acceptors.[12]

Starting from the dihydrogen molecule, H_2, there are several ways in which H–H bond activation can be accomplished. Both cationic centers and transition-metal centers are capable of this. For example, addition of H_2 to the methyl cation leads to the highly fluxional CH_5^+ molecule. At its potential energy minimum this molecule has a H–H bond length that is 0.2 Å longer than that in H_2 itself.[13]

Some transition metals form dihydride complexes and some $^2\eta$-H_2 complexes, and some form both, while there is strong evidence in favor of intermediate forms between these extremes.[14] H_2 bond activation can even be achieved without transition metals.[15] Very recently, Welch et al.[16] reported reversible dihydrogen activation using a phosphine-borane system. It is interesting to notice the resemblance between this system and the dihydrogen bonds discussed above. Similar dipolar H_2 activation is even believed to occur in metal-free hydrogenases.[17]

A novel mode of dihydrogen bonding was recently reported by Rauk and Armstrong in a computational study.[18] Despite the fact that neither HCl nor HBr have positive values of their electron affinities, they are both able to bind an electron in their dimeric forms, $[X{-}H{-}H{-}X]^-$ (X = Cl, Br). By adapting this symmetric bonding arrangement the dimers become thermodynamically stable. In addition, the authors noted a considerable lengthening of the X–H bond and correspondingly short H–H contacts (0.98 Å and 0.92 Å).[18] These are indeed noticeable features, and we observed the same phenomenon while sidetracking from work with one-electron reduction processes in water clusters and multiply protonated peptides. From our own quantum chemical calculations of analogous systems it turned out that HCl and HBr are the only neutral hydrides of rows 2, 3, and 4 of the periodic table capable of this type of bonding, meaning that although minimum energy structures of this kind can also be located for dimeric anions $[H_{n-1}E{-}H{-}H{-}EH_{n-1}]^-$ ($EH_n = PH_3$, AsH_3, H_2S, H_2Se, HF) they are thermodynamically unstable towards dissociation into the constituent monomers plus an electron, while for $EH_n = NH_3$, H_2O, there is no significant H–H bond.[19]

However, these endeavours led us to discover a new class of molecules, radical cations, also dimeric, and isoelectronic with the anions described above. In this paper we report the structures and properties of molecules of the type $[H_nE{-}H{-}H{-}EH_n]^+$. In contrast to their anionic counterparts, the cations constitute potential energy minima for all elements E belonging to Groups 15–18. As will become evident, their geometrical and electronic structures show clear periodic trends, and these trends can easily be understood from simple bond analyses. Furthermore, and probably of greatest significance, the periodic variations in binding illustrate a continuous spectrum of H_2 activation ranging from nonpolar covalent H–H to weak nonpolar H···H dihydrogen bonding.

Results and Discussion

All $[H_nE{-}H{-}H{-}EH_n]^+$ molecules listed in Table 1 and shown in Figure 1 adopt centrosymmetrical minimum energy structures. On the basis of experience[18,19] with the quantum chemical description of the isolectronic anions $[H_{n-1}E{-}H{-}H{-}EH_{n-1}]^-$, we expected UMP2/6–311+G(d,p) to provide accurate geometries and electronic structures also for the cations, since the cations, in contrast to the anions, are strongly electron binding in the sense that the highest (singly) occupied orbital always has an energy of −0.32 Hartrees or less.

However, we found it safe to check this assumption by performing additional CCSD(T)/def2–TZVPP calculations for the Group 18 molecules. The noble gas compounds were chosen because they have the weakest interaction between the element E and the central H_2 moiety and thereby were assumed to be most vulnerable to deficiencies in the wave function. Besides, they all belong to a computationally favorable molecular point group ($D_{\infty h}$). As one can see from Table 1 and Figure 1, the two levels of theory provide results that agree very well. In addition, we also wanted to assure ourselves that using one-determinant based wave functions was adequate. The UMP2 calculations for $H_2S{-}H{-}H{-}SH_2^+$ and $H_2Se{-}H{-}H{-}SeH_2^+$ gave slightly spin-contaminated wave functions from the UMP2 calculations with values of s(s+1) of 0.78 and 0.79, respectively. These two cations were chosen as candidates for CASSCF calculations together with the anion $Br{-}H{-}H{-}Br^-$. We found no instance in which the CI coefficient of the anticipated ground state configuration amounted to less than 0.97.

Table 1. Geometric structure data for $[H_nE\text{-}H\text{-}H\text{-}EH_n]^+$. (E = N, P, As, O, S, Se, F, Cl, Br, He, Ne, Ar, Kr, Xe). Bond lengths r in Å, vibrational frequencies υ in cm^{-1}. MP2 stands for MP2/6–311+G(d,p) (for H_nE = Xe it means MP2/def2-TZVPP), and CCSD(T) stands for CCSD(T)/def2-TZVPP.

H_nE	Point group	$r°$(EH)[a]	$r°$(EH)[b]		r(EH)[c]		r(HH)		υ(HH)	
		MP2	MP2	CCSD(T)	MP2	CCSD(T)	MP2	CCSD(T)	MP2	CCSD(T)
H_3N	D_{3d}	1.01	1.02	–	1.08	–	2.17	–	2225	–
H_3P	D_{3d}	1.41	1.39	–	1.85	–	0.94	–	1881	–
H_3As	C_2	1.51	1.48	–	2.01	–	0.88	–	2349	–
H_2O	C_2	0.96	0.98	–	1.25	–	1.17	–	1680	–
H_2S	C_2	1.33	1.35	–	1.82	–	0.90	–	2176	–
H_2Se	C_{2h}	1.46	1.47	–	2.04	–	0.84	–	2794	–
HF	C_2	0.92	0.96	–	1.27	–	1.08	–	2134	–
HCl	C_2	1.27	1.30	–	1.68	–	0.95	–	2094	–
HBr	C_2	1.41	1.44	–	1.88	–	0.89	–	2376	–
He	$D_{\infty h}$	–	0.79	0.78	1.27	1.24	1.05	1.06	2398	2339
Ne	$D_{\infty h}$	–	0.99	0.99	1.42	1.38	1.05	1.06	2398	2371
Ar	$D_{\infty h}$	–	1.28	1.28	1.63	1.64	1.00	1.00	2285	2277
Kr	$D_{\infty h}$	–	1.42	1.42	1.81	1.81	0.94	0.94	2326	2334
Xe	$D_{\infty h}$	–	1.60	1.60	2.03	2.05	0.86	0.86	2641	2640

[a] The bond length between E and H in H_nE. [b] The central bond length between E and H in $H_{n+1}E^+$. [c] The E–H bond length in $[H_nE\text{-}H\text{-}H\text{-}EH_n]^+$.

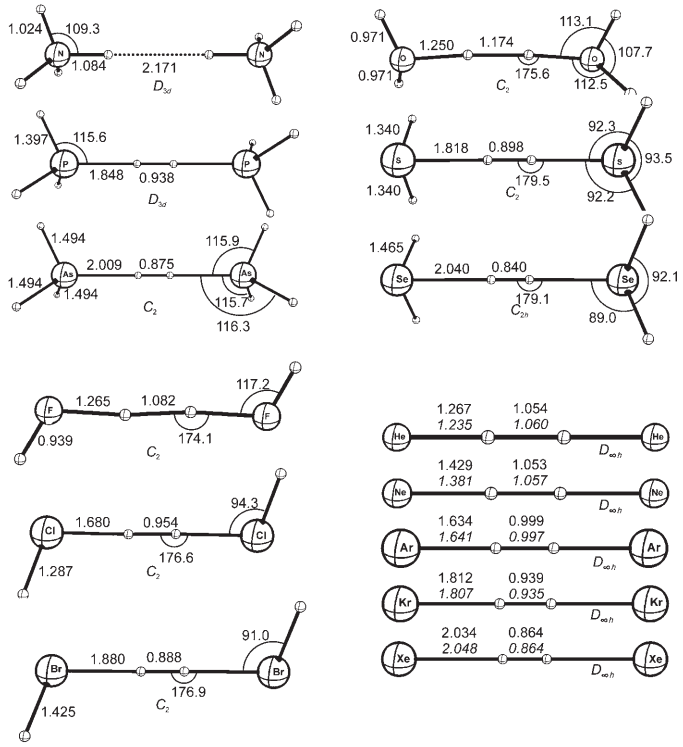

Figure 1. Optimized geometries (MP2/6–311+G(d,p) and *CCSD(T)/def2-TZVPP*) of $[H_nE\text{-}H\text{-}H\text{-}EH_n]^+$. Distances in Å, angles in degrees. The point group symmetry is given below each structure.

The analogy between the present dimeric radical cations and the aforementioned $Br\text{-}H\text{-}H\text{-}Br^-$ and $Cl\text{-}H\text{-}H\text{-}Cl^-$ systems is clear from an inspection of the bond distances. For example, the H–H bond distances for these molecules are 0.94 and 0.96 Å, respectively, which are close to the values for $KrHHKr^+$ (0.94 Å) and $ArHHAr^+$ (1.00 Å). In analogy with the anions, we may consider the $[H_nE\text{-}H\text{-}H\text{-}EH_n]^+$ dimer to be composed of two $H_nE\text{–}H^+$ molecules plus an electron. In that sense we observe, as for the hydrogen halide dimer anions,[18] a significant lengthening of the centrally pointing E–H bond in going from the monomer $H_{n+1}E^+$ to the electron-bound dimer $[H_nE\text{-}H\text{-}H\text{-}EH_n]^+$, see columns 4–7 of Table 1. For all E except E = N and E = He, the lengthening is between 27 and 43 %. In the nitrogen containing species the centrally pointing E–H bond is only 6 % longer, whereas for E = He we observe a dramatic bond elongation of 61 %. We note that such lengthening is characteristic for any acid forming a hydrogen bond towards any base, A–H···B. The degree of proton transfer in such cases depends on the acidity of A and the basicity of B. This picture is consistent with the observation that only the strongest acids, HCl and HBr, are able to give stabilized anionic dimers.

In concert with the E–H bond elongation of the centrally pointing E–H bond found for all $[H_nE\text{-}H\text{-}H\text{-}EH_n]^+$, we observe a complementary shortening of r(HH), the contact between the two bridging hydrogens (see Figure 1 and Table 1). This contact becomes shorter in going down the periodic table, but with no general trend left/right, except for the second row elements (N–Ne) for which r(HH) decreases from left to right. With the exception only of E = N, the H–H distances are much shorter than what is typical for polar dihydrogen bonds (see the Introduction). We also note the wide variation in this parameter, r(HH), ranging from 0.84 to 2.17 Å.

It is tempting to cite the harmonic vibrational frequencies corresponding to the symmetrical H–H stretching motion of the central moiety as a measure for the character of the H–H interaction. But as seen from the data in Table 1, there is no clear correlation between this quantity and the other properties listed in Tables 1–3, for example r(HH). The reason is simple. While the atoms in free H_2 (υ(HH) = 4533 cm^{-1}) and H_2^+ (υ(HH) = 3299 cm^{-1}) move in simple harmonic patterns, vibrations in $[H_nE\text{-}H\text{-}H\text{-}EH_n]^+$ represent heavily coupled motion. It is evident from the normal coordinate analysis that no sharp distinction can be made between the contribution from the E–H bond and the H–H

bond itself in the symmetrical stretching of the central H–H bond. The complex mechanical entanglement between these two bond stretching modes wipes out any simple physicochemical relationship between frequencies/force constants and related molecular properties.

It is interesting to compare the equilibrium H–H bond distances of the $[H_nE\text{-}H\text{-}H\text{-}EH_n]^+$ systems with the corresponding values in H_2 (0.74 Å at MP2/6–311+G(d,p)) and H_2^+ (1.05 Å at MP2/6–311+G(d,p)). The majority of the radical cations have H–H distances between these two prototypes. This observation points to an alternative description of the $[H_nE\text{-}H\text{-}H\text{-}EH_n]^+$ systems: instead of electron bond dimers ($2 \times H_nE{-}H^+ + e^-$) one may regard them as being composed of a H_2^+ molecule that is stabilized by two H_nE moieties. Before working out a detailed bonding scheme for the $[H_nE\text{-}H\text{-}H\text{-}EH_n]^+$ systems we concentrate on the question of whether such systems are likely to be observed experimentally.

Since all $[H_nE\text{-}H\text{-}H\text{-}EH_n]^+$ moieties correspond to local minima on their respective potential energy surfaces the prospect of experimental observation appears good provided they have sufficient thermochemical and kinetic stability. To assess this question we performed a series of calculations. We have identified the two most favorable decomposition pathways to be loss of H_2 and loss of H, as illustrated in Equations (1) and (2).

$$[H_nE\text{-}H\text{-}H\text{-}EH_n]^+ \rightarrow E_2H_{2n}^+ + H_2 \quad \Delta E_0(H_2\ \text{loss}) \qquad (1)$$

$$[H_nE\text{-}H\text{-}H\text{-}EH_n]^+ \rightarrow H_nE\cdots H\cdots EH_n^+ + H \quad \Delta E_0(H\ \text{loss}) \qquad (2)$$

For all second-row elements E except Ne the structure of $E_2H_{2n}^+$ is a dihydrogen bonded dimer between EH_{n+1}^+ and EH_{n-1} (see Figure 2). The heavier congeners prefer structures with a weak E–E bond. This is in agreement with Drewello et al., who find for E=S that forming an S–S bond gives a more stable arrangement for the dimer than forming a hydrogen bond.[20]

All noble gases form quite stable dimer radical cations, E_2^+, by similar binding arrangements. The general trend in the ΔE_0 data (column 5, Table 2), shows that dehydrogenation according to Equation (3) becomes thermochemically more advantageous the further one moves in the periodic table. For the second row analogues (N–Ne) plus all noble gases except Xe, the reaction is thermoneutral or endothermic. Dissociation via the alternative H loss route to give the proton bound dimer [Eq. (4)], shows the opposite periodic trend. With the exception of N–Ne plus Cl, all dimers are stable toward this dissociation. This means that the noble gases in terms of thermochemical stability show most overall promise as candidates for experimental observation.

Although a given radical cation dimer is thermochemically unstable from these considerations, it may still be amenable to observation provided the corresponding energy barrier ($\Delta E_0^{\neq}$) is sufficiently high. We therefore localized the transition structures for the dissociation reactions, applying the systematic approach described in the Methods section.

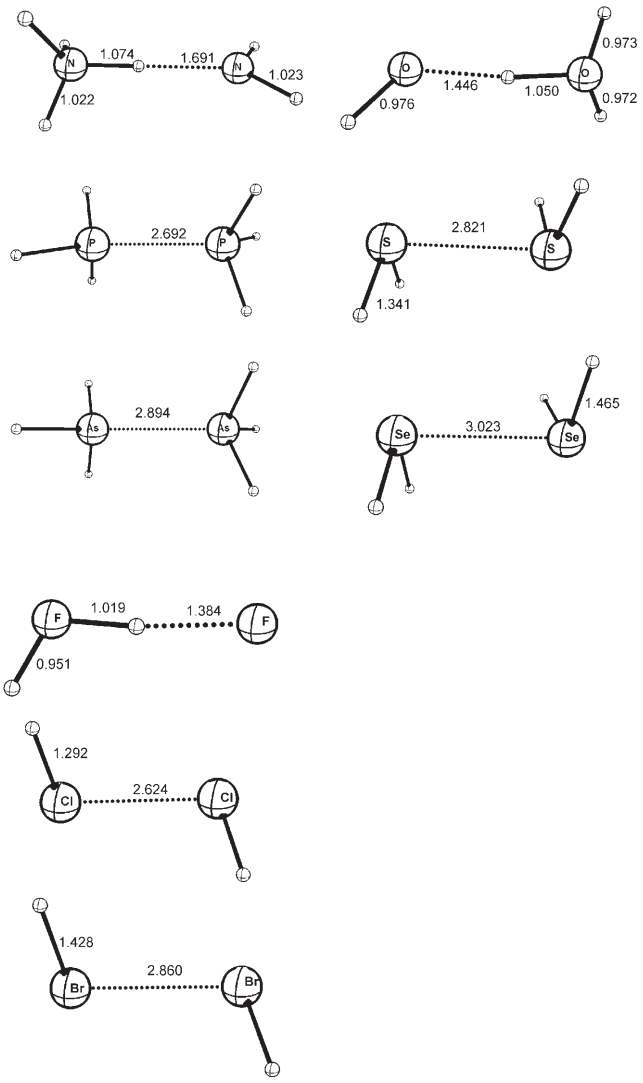

Figure 2. Optimized geometries (MP2/6–311+G(d,p)) for the products of H_2 loss $E_2H_{2n}^+$ (E=N, P, As, O, S, Se, F, Cl, Br). Distances in Å.

Figure 3 depicts the transition structures for loss of H_2 and H (except the noble gas compounds). For all cases, even for the most exothermic ones, the calculations showed there is a noticeable barrier towards H_2 loss (Table 2). We do, however, realize that in most cases (H_2O and NH_3 are clear exceptions) the barrier is probably too small to trap the dimer for an extended period of time at room temperature. Moreover, taking the atomic motions corresponding to the respective transition vectors into account (mostly hydrogen movements) tunnelling will effectively lower the activation energy below the listed activation energy values $\Delta E_0^{\neq}$. For the noble gases, the found transition structures turned out not to connect to the loosely bounded intermediate $E_2^+\cdots H_2$ as for the other Groups 15–17. Instead, the connected product is $E\cdots EH_2^+$ (Figure 4). In order to make this distinction in the mechanism we have termed this dissociation alterna-

Table 2. Energy data for $[H_nE\text{-}H\text{-}H\text{-}EH_n]^+$ in kJ mol^{-1} including the zero point vibrational contribution. MP2/6–311+G(d,p) data unless otherwise indicated. CCSD(T)/def2-TZVPP values are given in parentheses.[a]

H_nE	E_{ea}[b]	E_{com}[c]	PA[d]	ΔE_0 H_2 loss[f]	$\Delta E_0^{\neq}$ H_2 loss[h]	ΔE_0 rearr[i]	$\Delta E_0^{\neq}$ rearr[j]	ΔE_0 H loss[k]	$\Delta E_0^{\neq}$ H loss[l]
H_3N	515	664	854	0	132			−58	22
H_3P	560	597	785	−63	38			12	35
H_3As	611	575	763	−80	21			33	56
H_2O	684	501	689	56	74			−86	13
H_2S	677	549	708	−59	41			26	61
H_2Se	709	576	715	−80	27			52	91
HF	895	296	486	179	–			−68	6
HCl	813	383	563	−1	–			−5	41
HBr	821	401	586	−45	46			27	–
He	1240	28	177[e]	686		1	1	52	–
	(1235)	(23)		(679)				(53)	
Ne	1207	35	199[e]	522		1	1	36	–
	(1198)	(55)		(507)				(33)	
Ar	991	190	369[e]	112		24	25	2	–
	(1003)	(209)		(107)				(15)	
Kr	973	249	424[e]	24		42	45	21	–
	(976)	(278)		(25)				(37)	
Xe	936[g]	353[g]	500[e]	−36[g]		−36[g]	45[g]	55[g]	n.c.
	(936)	(376)		(−37)				(71)	

[a] No entry means does not apply, hyphen means not found, and n.c. means not calculated. [b] Gain in energy for 2 $H_nEH^+ + e^- \rightarrow [H_nE\text{-}H\text{-}H\text{-}EH_n]^+$. [c] Gain in energy for 2 $H_nE + H_2^+ \rightarrow [H_nE\text{-}H\text{-}H\text{-}EH_n]^+$. [d] Proton affinity, data from ref. [39]. [e] Data from ref. [40]. [f] Energy of reaction for $H_nE\text{-}H\text{-}H\text{-}EH_n^+ \rightarrow E_2H_{2n}^+ + H_2$. [g] Calculated using the def2-TZVPP basis set. [h] 0 K activation energy for $[H_nE\text{-}H\text{-}H\text{-}EH_n]^+ \rightarrow E_2H_{2n}^+ + H_2$. [i] Energy of reaction for $E\text{-}H\text{-}H\text{-}E^+ \rightarrow E_2\text{-}H\text{-}H^+$. [j] 0 K activation energy $E\text{-}H\text{-}H\text{-}E^+ \rightarrow E_2\text{-}H\text{-}H^+$. [k] Energy of reaction for $[H_nE\text{-}H\text{-}H\text{-}EH_n]^+ \rightarrow [H_nE\text{-}H\text{-}EH_n]^+ + H$. [l] 0 K activation energy for $[H_nE\text{-}H\text{-}EH_n]^+ \rightarrow [H_nE\text{-}H\text{-}EH_n]^+ + H$.

tive "rearr" in Table 2. The dimers are both thermochemically and kinetically stable towards this rearrangement mechanism (except for Xe which is only kinetically stable). The transition structures for H loss also give definite values for $\Delta E_0^{\neq}$ but also in this case some of the barriers may be sufficient for long-time trapping under thermal conditions. Unfortunately, the trends in barrier heights for H and H_2 are opposite. The two species $H_3N\text{-}H\text{-}H\text{-}NH_3^+$ and $H_2O\text{-}H\text{-}H\text{-}OH_2^+$, which both were found to be kinetically stable towards H_2 loss, have barriers for H loss of only 22 and 13 kJ mol^{-1}, respectively. We must therefore conclude that the species that are thermochemically unstable, are most likely to be kinetically unstable too. This leaves us with the radical cations derived from the noble gases as being most easily accessible for straightforward structural or spectroscopic observation.

How can we rationalize the structures and stabilities of the $[H_nE\text{-}H\text{-}H\text{-}EH]^+$ systems? Are they electron-bound dimers of two H_nE^+ units or should they be described as adducts between H_2^+ and two H_nE moieties? Can we understand which factors govern the fine tuning of the H···H interaction? We will address these questions by analyzing the energetics and the charge distributions by means of a charge decomposition method and in terms of frontier orbital arguments.

The geometrical data lead us to two different perspectives for understanding the bonding patterns in $[H_nE\text{-}H\text{-}H\text{-}EH_n]^+$ in general: from the first perspective two EH_n units stabilize a H_2^+ moiety, and from the second an electron binds two H_nEH^+ units. Starting with the notion that the present molecules may be regarded as a combination of two cations (e.g. two ammonium ions) with an electron, we define the associated energy of reaction, given in Equation (3).

$$2\,H_nEH^+ + e^- \rightarrow [H_nE\text{-}H\text{-}H\text{-}EH_n]^+ \quad -E_{ea} \tag{3}$$

Equivalently, we identify the reverse reaction as a dissociative second ionization of $H_nE\text{-}H\text{-}H\text{-}EH_n^+$. From this latter consideration we may understand the increase in E_{ea} from left to right in the periodic table as a reflection of the matching increase in the ionization energy (*IE*) of the central element. There is, however, no similar trend upon moving downwards within one group.

We may understand this lack of correlation as resulting from the fact that a strong central dihydrogen bond is formed, a tendency that is enhanced upon moving downwards and which is also reflected in the decreasing H–H bond length r(HH) (Table 1). In particular the very high E_{ea} value for E = He for example, can be rationalized when taking into account that the H–H bond length r(HH) in $He\text{-}H\text{-}H\text{-}He^+$ matches the value for free H_2^+ (1.05 Å), whereas the He–H bond is noticeably elongated by 61% compared to $He\text{–}H^+$. We note that the E_{ea} value for $He\text{-}H\text{-}H\text{-}He^+$ of 1240 kJ mol^{-1} is rather close to the total energy of H_2^+ itself ($2\,H^+ + e^- \rightarrow H_2^+$ E = 1579 kJ mol^{-1} at MP2/6–311+G(d,p)).

Alternatively, as stated above, one may analyze the electronic structure in view of an association between two neutral molecules and a central H_2^+ molecule, as shown in Equation (4).

$$2\,H_nE + H_2^+ \rightarrow [H_nE\text{-}H\text{-}H\text{-}EH_n]^+ \quad -E_{com} \tag{4}$$

Table 2 shows how this quantity reflects the properties of the element hydrides, EH_n. This becomes even more apparent by plotting E_{com} against the proton affinity (*PA*), which reveals a good linear correlation (Figure 5).

Proton affinity is a measure of a molecule's ability to bind a proton. Upon binding the proton, electron density is donated from H_nE into the region of bond formation $H_nE\text{–}H^+$. Among other factors, ionization energy and molecular polarizability are important in determining the char-

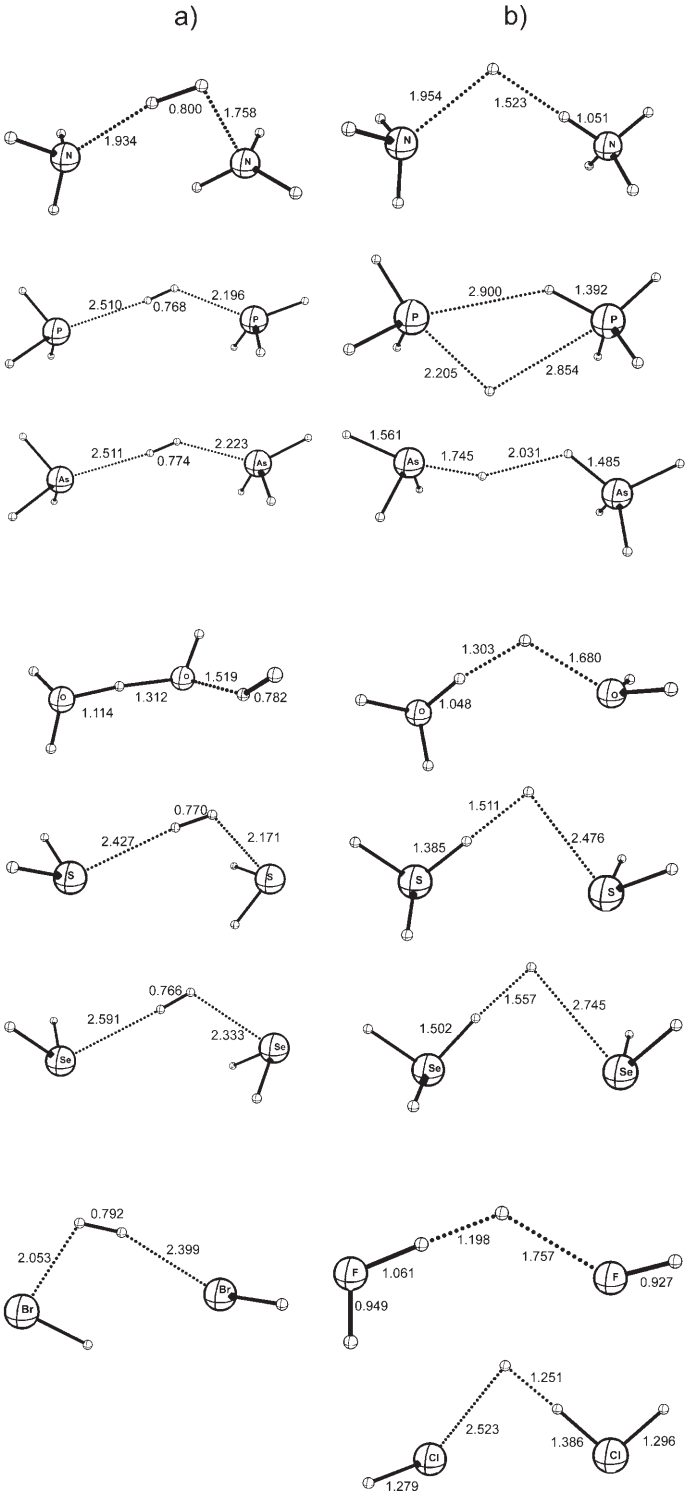

Figure 3. Transition structures for the loss of a) H_2 and b) H.

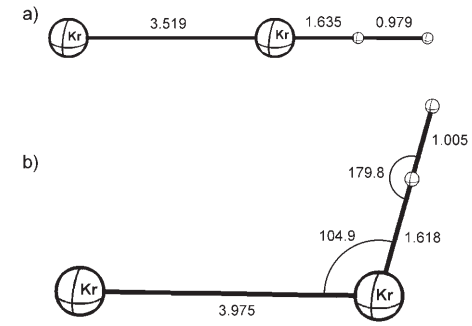

Figure 4. a) Product and b) transition state structures for the rearrangement reaction of the noble gas compounds E-H-H-E^+ → E···EH_2^+ (exemplified for E = Kr). Distances in Å, angles in degrees.

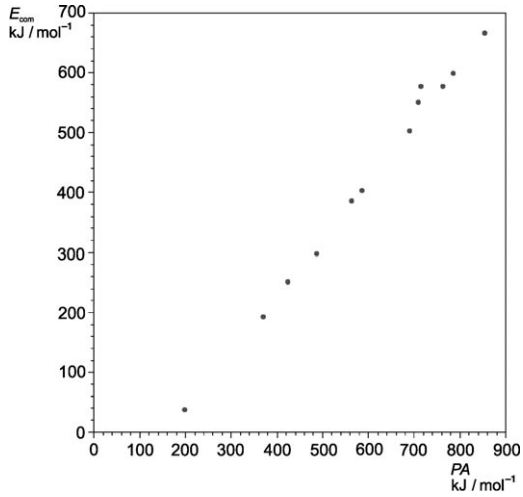

Figure 5. The relationship between the negative binding energy for the association reaction $2H_nE + H_2^+ \rightarrow [H_nE\text{-}H\text{-}H\text{-}EH_n]^+$ (E_{com}) and the proton affinity (PA) of EH_n. ($E_{com} = 0.970PA - 156$; $r^{2=}0.993$).

acteristic periodic variation in PA.[21] The value of PA decreases from left to right, while it decreases down Group 15 but increases down Groups 16, 17, and 18, most noticeably for the latter. Quite similar mechanisms for electron transfer are evidently in operation during formation of both $H_nE{-}H^+$ and $[H_nE\text{-}H\text{-}H\text{-}EH_n]^+$. There are, however, two noticeable differences: the total interaction is weaker in the latter case, despite the fact that there are two H_nE molecules involved, and electron density is not only limited to the E–H region but may enter into or even be removed from the H–H region as well. These latter abilities are not supported by a large value of the proton affinity. The example of $H_3N\text{-}H\text{-}H\text{-}NH_3^+$ illustrates this elegantly. The strongest base in our data set, NH_3, has the largest value of E_{com}, but also a very large r(HH) value of 2.17 Å. This means that the H_2^+ unit dissociates when it is attached to two NH_3 molecules, and one has to keep in mind that the E_{com} value includes the dissociation energy of the H_2^+ ion of 266 kJ mol^{-1}.

It is interesting that a few systems adopt the $[H_nE{-}H\cdots H{-}EH_n]^+$ structure which is best described as a weakly bound electron-bound dimer of EH_{n+1}^+, and others show a shorter but variable central H–H bond in the structural motif $[H_nE\cdots H{-}H\cdots EH_n]^+$. In order to come to an understanding of the underlying bonding patterns we plotted the potential energy variation upon stretching of the central H–H bond r(HH) for the Group 15–18 systems [The curves for E = F and E = S are not shown, since the relaxed scans for large

r(HH) lead to structures of completely different topologies (H loss)] (Figure 6). The shape of the energy curves for E = P, As, Se, Cl, Br, and the noble gases are very similar to the curve for an isolated H_2^+ system. This similarity shows that the driving force in these systems is indeed the formation of a strong covalent H–H bond like in H_2^+. The details of the dissociation curve (well depth and equilibrium distance) are moderated by the nature of EH_n, as will be discussed below. The curves for E = O and N differ from the rest, since they are considerably flatter, reflecting the $[H_nE–H\cdots H–EH_n]^+$ character.

In the case of E = N this formulation is completely dominating, since the energy minimum structure has a particularly extended r(HH). However, we note a flattening of the potential energy curve for H_3N-H-H-NH_3^+ in the range of r(HH) ≈ 1.2 Å which reflects the tendency for H–H bond formation.

The partial charges q for the centrally pointing hydrogen, q(H), and the element q(E) of the $[H_nE$-H-H-$EH_n]^+$ systems are given in Table 3. They show absolutely regular trends, as the partial charges of the central element q(E) increase and the charge of the centrally pointing H atom q(H) decreases when going down Groups 15–17. More informative is the comparison of the charge difference between the central and the terminal hydrogen atoms, Δq(H). It indicates that there is an upsurge of electron density in the region around the two central hydrogen atoms at the expense of the terminal ones. The value of this parameter does not tell which part of the region between the E atoms (E–H or H–H) accommodates the surplus electron density, but it is essential that a negative value of Δq(H) is found, irrespective of the length of the H–H bond. This supports the view that the radical cations can be regarded as electron-bound dimers of two $H_nE–H^+$ cations. However, the partial charges do not reflect the fundamental change in the bonding situation upon going from H_3N-H-H-NH_3^+ to H_3P-H-H-PH_3^+. The plot of the electron density distribution $\rho(r)$ along the E-H-H-E paths (see Figure 7) and the value of $\rho(r_{crit})$ and its laplacian $\nabla^2\rho(r_{crit})$ at the central bond critical point r_{crit} (Table 3) are more instructive. The magnitude of $\rho(r_{crit})$ is

Table 3. Calculated (NBO) Partial Charges q(X) of the atoms X and the one-electron density (ρ) and its Laplacian ($\nabla^2\rho$) at the central bond critical point r_{crit} for $[H_nE$-H-H-$EH_n]^+$ at the MP2/6–311+G(d,p) level. All values in atomic units.

H_nE	q(E)[a]	q(H)[b]	Δq(H)[c]	$\rho(r_{crit})$	$\nabla^2\rho(r_{crit})$
H_3N	−0.94	0.16	−0.27	0.02	0.00
H_3P	0.39	−0.01	−0.05	0.14	−0.38
H_3As	0.43	−0.01	−0.04	0.15	−0.33
H_2O	−0.79	0.24	−0.29	0.09	−0.18
H_2S	0.15	0.02	−0.15	0.16	−0.46
H_2Se	0.26	−0.01	−0.12	0.19	−0.61
HF	−0.43	0.31	−0.31	0.10	−0.29
HCl	0.09	0.10	−0.21	0.13	−0.37
HBr	0.22	0.05	−0.22	0.17	−0.48
He	0.08	0.42	–	0.09	−0.36
Ne	0.09	0.41	–	0.10	−0.35
Ar	0.29	0.21	–	0.12	−0.34
Kr	0.36	0.14	–	0.14	−0.45

[a] NBO charge for each E. [b] NBO charge for each bridging hydrogen atom. [c] Charge difference between one central H and one terminal hydrogen atom.

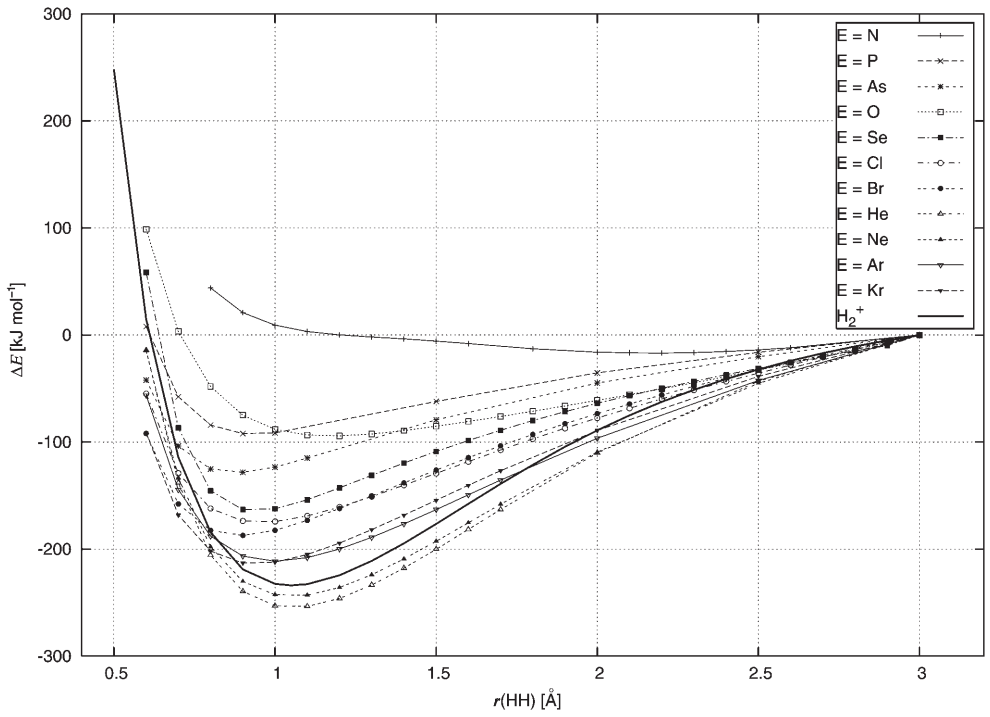

Figure 6. Change in energy of the $[H_nE$-H-H-$EH_n]^+$ systems (E = N, P, As, O, Se, Cl, Br, He, Ne, Ar, Kr) upon changing the central H–H bond length r(HH). For comparison the corresponding curve for the H_2^+ system is also given. All values on the MP2/6–311+G(d,p) level.

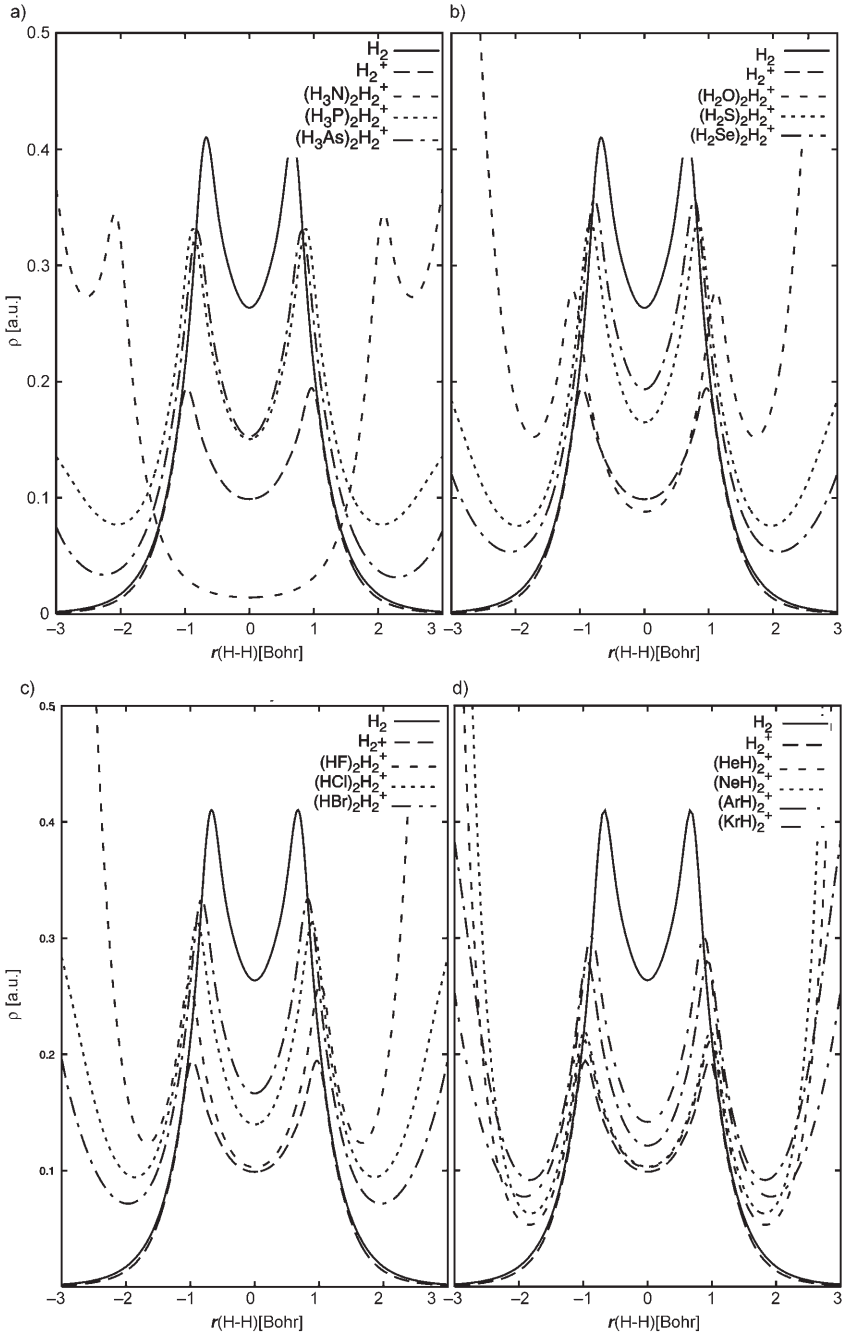

Figure 7. Electron density distribution $\rho(r)$ along the E-H-H-E paths in $[H_nE\text{-}H\text{-}H\text{-}EH_n]^+$ for a) Group 15, b) Group 16, c) Group 17 and d) Group 18 elements. All values on the MP2/6–311+G(d,p) level.

indicative of the extent of bonding. For H_2 and H_2^+ the bond critical points are midway between the hydrogen atoms, and $\rho(\boldsymbol{r}_{crit})$ is 0.26 a.u. and 0.09. a.u, respectively. Two features appear. Firstly, for all radical cations except E=N there is sizeable electron density in the region between the two central hydrogen nuclei. Secondly, there is good correlation between the value of the electron density at the central bond critical point and the H–H bond length: the shorter $\boldsymbol{r}$(HH) the higher is $\rho(\boldsymbol{r}_{crit})$. Not unexpectedly, the radical cations with the lowest $\rho(\boldsymbol{r}_{crit})$, longest $\boldsymbol{r}$(HH) and shortest $\boldsymbol{r}$(EH) (namely H_nE=HF, H_2O and NH_3) all have significantly higher electron density in the E–H region than the others. This may account for their highly negative Δq(H) values, as noted above. It is also worth noting that, with the exception of E=N, the Laplacian of the electron density, $\nabla^2\rho$, always has a significantly negative value at the H–H bond critical point. This is often interpreted as a signature of a covalent bond. The corresponding values for the Laplacian, $\nabla^2\rho(\boldsymbol{r}_{crit})$, of H_2 and H_2^+ are −1.08 a.u. and −0.36 a.u., showing that in many cases the central H–H bond, using this criterion, can be considered to be between these two. There is (not shown here) close resemblance between the $\rho(\boldsymbol{r})$ distributions for $BrHHBr^-$ and $KrHHKr^+$ and between $ClHHCl^-$ and $ArHHAr^+$.

In concluding this section, we analyze the gliding scales of H–H and E–H interactions within $[H_nE\cdots H\text{-}H\cdots EH_n]^+$ in terms of orbital interactions. Our analysis represents an *a posteriori* rationalization, but contains valuable qualitative insight into the bonding situation. The discussion is illustrated with the two orbital diagrams shown in Figures 8 and 9.

We start from the hypothetical system $[H_nE\text{-}H\text{-}H\text{-}EH_n]^+$ with equal bond length and nonpolar H_nE–H bonds (Figure 8, middle). The completely symmetric combination of the atomic orbitals leads to the energetically lowest orbital σ_1, followed by σ_2 with one node which is E–H bonding and H–H antibonding and σ_3 with two nodes that has H–H bonding and E–H antibonding character. These three orbitals are occupied by a total of five electrons, whereas the totally antisymmetric orbital σ_4 remains empty. Through a shortening of the E–H bond and a lengthening of the H–H bond (Figure 8 right) the σ_1 and σ_2 orbitals become stabilized, whereas σ_3 and σ_4 increase in energy. The alternative distortion (Figure 8, left) with a decreasing H–H bond length and an increased E–H bond distance stabilizes the σ_1

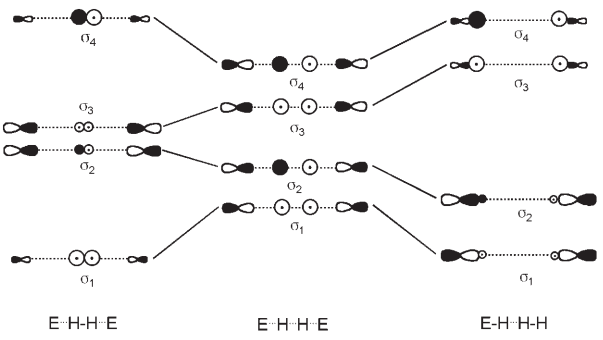

Figure 8. Schematic sketch of the four-center, five-electron σ-bonding in the systems $[H_nE\text{-}H\text{-}H\text{-}EH_n]^+$. In the middle a hypothetical nonpolar system with equal E–H and H–H bond lengths is drawn. The influence of the shortening of the central H–H bond for an electropositive E on the orbital structure is given on the left. The shortening of the E–H bond for electronegative E is shown on the right.

and the σ_3 orbitals and destabilizes the σ_2 and σ_4 orbitals. The answer to the question of which of the two distortive modes a given compound will choose, depends, in our simple bonding model, mainly on the strength of the H_nE–H and H–H bonds and on the polarity of the H_nE–H bond. If the H_nE–H bond is very strong and the H_nE group is very electronegative, distortion toward H_nE–H···H–EH_n will result, since the H_nE orbitals dominate the low-lying doubly occupied orbitals σ_1 and σ_2 (Figure 8, right). In contrast to this, a more electropositive H_nE and/or a weaker H_nE–H bond can lead to the H_nE···H–H···EH_n structure (Figure 8 left), since the doubly occupied orbitals are dominated by the contributions of the central hydrogen atoms. It is not possible to predict from this simple orbital picture which structure type will be realized, since there is an intricate interplay between the strength of the H_nE–H bonds, the H–H interaction and the total delocalisation of the electronic charge. However, the fine tuning of the H–H interaction can easily be rationalized once the structure type is known. In Figure 9 we give an orbital interaction diagram for bonding in $[H_nE\cdots H\text{–}H\cdots EH_n]^+$ which we regard as being composed of H_2^+ and two H_nE units.

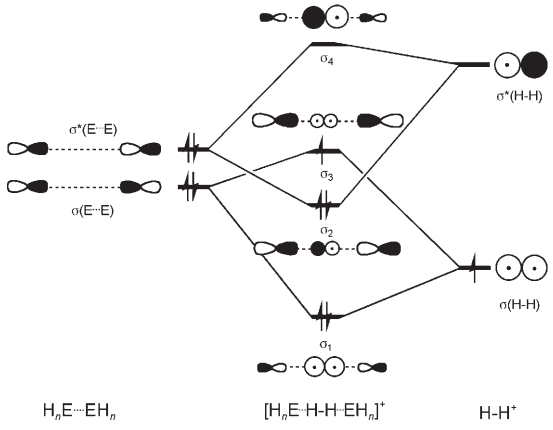

Figure 9. Schematic orbital interaction diagram for the interaction of H_2^+ with two EH_n leading to $[H_nE\cdots H\text{–}H\cdots EH_n]^+$.

The decisive point for the fine tuning of the H–H interaction is the orbital energy of the EH_n σ-orbitals σ(E···E) and σ^*(E···E) (Figure 9). The higher these orbitals are in energy the less they contribute to the σ_1 orbital of $[H_nE\cdots H\text{–}H\cdots EH_n]^+$. This means that the H–H interaction becomes stronger and more charge will be donated from the H_nE onto the H_2^+ moiety. The stabilisation of the H–H bonding is enhanced by the singly occupied σ_3 orbital. To a certain extent these stabilizing effects are counterbalanced by the H–H antibonding orbital σ_3 to which the H_2^+ fragment orbitals will contribute more the higher the orbitals of H_nE are in energy. This bonding scheme suggests that the H–H bond has more two-electron character the higher lying are the σ-orbitals of EH_n. The orbital energies of the H_nE units increase upon moving down the periodic table, in accord with the decreasing bond length of the H–H bond and the increasing partial charges of the centrally pointing H atoms in the $[H_nE\cdots H\text{–}H\cdots EH_n]^+$ systems when going down the groups.

Conclusion and Perspective

The most pertinent finding of this study is of fundamental character. The new family of species $[H_nE\text{-}H\text{-}H\text{-}EH_n]^+$ comprises full variation of H_2 activation ranging from purely covalent H–H character to the extremely weak H···H interaction. While H_2 and H_2^+ are the classical textbook examples of two-electron and one-electron bonds, the present molecules represent a continuous spectrum between two- and zero-electron bonds. We have described the periodic trends in binding and electron structure of $[H_nE\text{-}H\text{-}H\text{-}EH_n]^+$ in detail, and (in hindsight) shown how the well-known properties of the element hydrides, EH_n, govern binding. These trends are rationalized in terms of molecular orbital interactions.

As already mentioned the radical cations formed from the elements of Groups 15–17 probably do not possess sufficient thermochemical and kinetic stability in themselves to allow for isolation in the gas phase. Despite this, we see a potential for these types of structural motifs (not the actual molecules discussed in this article) as building blocks for solid-state devices for hydrogen storage. This will of course require some additional stabilization in the form of cage or lattice effects. On the other hand, the structures should not be too stabilized in favor of H_2 binding since H_2 should be easily liberated during use. In that respect, both neutral energetics and low barriers for decomposition are required. One parameter for the search for practically applicable systems could be the orbital energies of the σ-orbitals of the EH_n units since these influence the bonding situation to a high degree.

Irrespective of practical application, the species reported here may be of relevance for describing important redox processes in aqueous solutions and within living cells. Often

little is known about the detailed mechanisms associated with a wide collection of fast reactions usually described by Equation (5).

$$2\,H^+ + 2\,e^- \rightarrow H_2 \quad (5)$$

Some of the rather vulnerable species reported here for Groups 15–17 may be short-lived intermediates during such redox processes. Based upon these considerations, we may propose a general three-step mechanism to account for reactions of this kind. This mechanism is detailed in Equation (6a)–(6e), followed by either Equation (6c), or Equations (6d) and (6e).

$$H_nE{-}H^+ + e^- \rightarrow H_nE{-}H \quad (6a)$$

$$H_nE{-}H + H_nE{-}H^+ \rightarrow [H_nE\text{-}H\text{-}H\text{-}EH_n]^+ \quad (6b)$$

$$[H_nE\text{-}H\text{-}H\text{-}EH_n]^+ + e^- \rightarrow 2\,H_nE + H_2 \quad (6c)$$

$$[H_nE\text{-}H\text{-}H\text{-}EH_n]^+ \rightarrow E_2H_{2n}{}^+ + H_2 \quad (6d)$$

$$E_2H_{2n}{}^+ + e^- \rightarrow 2\,H_nE \quad (6e)$$

As discussed above, several of the dimers are not very stable towards H_2 loss. In these cases the lifetime of the intermediate $[H_nE\text{-}H\text{-}H\text{-}EH_n]^+$ may be too short to allow reduction by the second electron before dissociation, so the second electron will then correspond to reduction of the soformed $E_2H_{2n}{}^+$ species, in Equations (6d) and (6e). Very recently, Zubarev and co-workers reported that two hydrogen atoms, most likely in the form of a H_2 molecule, are lost upon electron capture dissociation of multiply protonated peptides. This observation may be accounted for by a reaction sequence analogous to Equations (6a), (6b), and (6d).[22]

The more stable E-H-H-EH$^+$ Group 18 compounds are probably not of great practical value. On the other hand, they allow direct laboratory observation. Since the helium and neon congeners are too weakly bonded, the hunt must be limited to Ar and Kr. Xenon has unfavorable thermochemistry since the H_2 rearrangement channel is slightly exothermic. Conducting ion molecule reactions in a selected ion flow tube Bedford and Smith demonstrated that it is possible to form $ArH_2{}^+$, by ligand switching from $Ar_2{}^+$.[23] The data of Table 2 indicate that this species, or more precisely the complex Ar···$ArH_2{}^+$, is considerably less strongly bonded than Ar-H-H-Ar$^+$. Therefore it should be possible, at least in principle, to make the latter in the third body stabilized reaction shown in Equation (7).

$$ArH_2{}^+ + Ar \rightarrow Ar\text{-}H\text{-}H\text{-}Ar^+ \quad (7)$$

This method appears even more attractive for Kr (and perhaps also Xe). To this end our own attempts, applying noble gas/dihydrogen mixtures under chemical ionization conditions, have been unsuccessful. Production of reaction plasma of the necessary chemical composition has been severely hampered by the presence of even trace amounts of water.

It could turn out to be more successful to look for the species in a frozen matrix of any of the same noble gases. Interstitial hydrogen molecules may then be brought to binding to matrix atoms subsequent to selective ionization [Eq. (8)]

$$Ar^+ \cdots H{-}H \cdots Ar \rightarrow Ar\text{-}H\text{-}H\text{-}Ar^+ \quad (8)$$

It may be favorable to use a noble gas of lower ionization energy than H_2 (Kr or Xe) to avoid bringing too much excitation energy into the reaction region. Radical cation formation may be monitored by electron spin resonance spectroscopy. Alternatively, infrared spectroscopy, for example to record the antisymmetric (E–H)str. combination could be used. The symmetric (H–H)str. is infrared inactive. There appear to have been only a few attempts to investigate chemical reactions initiated by radiation of noble gas/dihydrogen matrices.[24,25]

Methods

All structures (minima and transition structures) were subjected to full geometry optimization by applying unrestricted Møller–Plesset perturbation theory to second order[26] and a split valence Pople basis function augmented with polarization and diffuse functions,[27] UMP2/6–311+G-(d,p), using standard cut-off values. For each optimized geometry the force constant matrix (Hessian) was calculated and checked for the correct number of negative eigenvalues (0 for minima, 1 for transition structures), and harmonic vibrational frequencies were derived. Zero point vibrational correction to the energy was carried out applying these frequencies without scaling. Two complementary strategies for finding transition structures were chosen. The first was loosely based on normal coordinate following, starting from the minimum energy structure and identifying the lowest frequency vibrations corresponding to the out-of-axis vibrations of the central hydrogens. The second was of more pragmatic character in that a small set of likely transition structures were hand-picked to interconnect reactant and product structures. All candidate structures were then subjected to geometry optimization during which the Hessian (force constant matrix) was calculated analytically for each iterative step. All found transition structures were subjected to intrinsic reaction coordinate (IRC) calculation[28] with subsequent optimization of the end point geometries to ensure that the found TS connected the two anticipated minima. All these calculations were done with the Gaussian03 suite of programs.[29] To validate the use of one-determinant based wave functions, complete active space calculations[30] using a double zeta Dunning basis set,[31,32] CASSCF/cc-pVDZ, were performed for a couple of cases (see preceding text for more details). All dimers of Group 18 were reoptimized by the use of coupled cluster singles-doubles theory including a perturbative treatment of the triples amplitudes together with the Weigend-Ahlrichs all-electron basis,[33] CCSD(T)/def2-TZVPP, and vibrational frequencies were calculated. For Xe the effective core potential basis set ECP-28-MDF[34] was used in conjunction with the def2-TZVPP valence basis set.[33] Both CASSCF and CCSD(T) calculations were done with programs implemented in the Molpro package.[35] The MP2/6–311+G(d,p) one-electron densities were analyzed using the AIMPAC program by Bader and co-workers,[36,37] and natural bond orbital (NBO) charges were obtained using Weinhold's approach.[38]

[1] T. Richardson, S. de Gala, R. H. Crabtree, P. E. M. Siegbahn, *J. Am. Chem. Soc.* **1995**, *117*, 12875.
[2] W. H. Zachariasen, R. C. L. Mooney, *J. Chem. Phys.* **1934**, *2*, 34.
[3] A. P. Burg, *Inorg. Chem.* **1964**, *3*, 1325.

[4] M. P. Brown, R. W. Heseltine, *J. Chem. Soc. Chem. Commun.* **1968**, 1551.
[5] R. C. Stevens, R. Milstein, O. Blum, T. F. Koetzle, *J. Chem. Soc. Dalton Trans.* **1990**, 1429.
[6] R. H. Crabtree, P. E. M. Siegbahn, O. Eisenstein, A. L. Rheingold, T. F. Koetzle, *Acc. Chem. Res.* **1996**, *29*, 348.
[7] R. Custelclean, J. E. Jackson, *Chem. Rev.* **2001**, *101*, 1963.
[8] S. J. Grabowski, *J. Phys. Chem. A* **2000**, *104*, 5551.
[9] D. Hugas, S. Simon, M. Duran, *Struct. Chem.* **2005**, *16*, 257.
[10] W. Zierkiewicz, P. Hobza, *Phys. Chem. Chem. Phys.* **2004**, *6*, 5288.
[11] D. Cremer, E. Kraka, *J. Phys. Chem.* **1986**, *90*, 33.
[12] S. Hammerum, C. B. Nielsen, *J. Phys. Chem. A* **2005**, *109*, 12046.
[13] P. C. Hariharan, W. A. Lathan, J. A. Pople, *Chem. Phys. Lett.* **1972**, *14*, 385.
[14] G. J. Kubas, *Metal Dihydrogen and sigma-Bond Complexes*, Kluwer Academic/Plenum, New York, **2001**.
[15] E. Uggerud, *Mass Spectrom. Rev.* **1999**, *18*, 285.
[16] G. C. Welch, R. R. S. Juan, J. D. Masuda, D. W. Stephan, *Science* **2006**, *314*, 1124.
[17] A. P. Scott, B. T. Golding, L. Radom, *New J. Chem.* **1998**, *22,* 1171.
[18] A. Rauk, D. A. Armstrong, *J. Phys. Chem. A* **2002**, *106*, 400.
[19] E. Uggerud, unpublished data on calculations of $[H_nE\text{-}H\text{-}H\text{-}EH_n]^-$ (E = element of Groups 15–17) **2007**.
[20] T. Drewello, C. B. Lebrilla, H. Schwarz, L. J. d. Koning, R. H. Fokkens, N. M. M. Nibbering, E. Anklam, K.-D. Asmus, *J. Chem. Soc. Chem. Commun.* **1987**, 1381.
[21] E. Uggerud, *Mass Spectrom. Rev.* **1992**, *11*, 389.
[22] M. M. Savitski, F. Kjeldsen, M. L. Nielsen, R. A. Zubarev, *J. Am. Soc. Mass Spectrom.* **2007**, *18*, 113.
[23] D. K. Bedford, D. Smith, *Int. J. Mass Spectrom. Ion. Proc.* **1990**, *98*, 179.
[24] M. Beyer, E. V. Savchenko, G Niedner-Schattenburg, V. E. Bondybey, *Low Temp. Phys.* **1999**, *25*, 814.
[25] M. A. Pittman, J. J. Banisaukas, L. B. Knight, in *58th Southeast Regional Meeting of the American Chemical Society*, Augusta, GA, United States, November 1–4, **2006**, p. SRM06 777.
[26] C. Møller, M. S. Plesset, *Phys. Rev.* **1934**, *46*, 618.
[27] R. Krishnan, J. S. Binkley, R. Seeger, J. A. Pople, *J. Chem. Phys.* **1980**, *72*, 650.
[28] C. Gonzales, H. B. Schlegel, *J. Phys. Chem.* **1989**, *93*, 2154.
[29] M. J. Frisch, et al., Gaussian 03 Revision D.01, Gaussian Inc., **2004**.
[30] K. Andersson, P. A. Malmqvist, B. O. Roos, A. J. Sadlej, K. Wolinski, *J. Phys. Chem.* **1990**, *94*, 5483.
[31] T. H. Dunning, *J. Chem. Phys.* **1989**, *90*, 1007.
[32] D. E. Woon, T. H. Dunning, *J. Chem. Phys.* **1993**, *98*, 1358.
[33] F. Weigend, R. Ahlrichs, *Phys. Chem. Chem. Phys.* **2005**, *7*, 3297.
[34] K. A. Peterson, D. Figgen, E. Goll, H. Stoll, M. Dolg, *J. Chem. Phys.* **2003**, *119*, 11113.
[35] H.-J. Werner, P. J. Knowles, R. Lindh, F. R. Manby, M. Schütz, *MOLPRO*, *version 2006.1*, *a package of ab initio programs*, *see http://www.molpro.net*.
[36] R. F. W. Bader, *Atoms in Molecules. A Quantum Theory*, Oxford Press, Oxford, **1990**.
[37] R. W. F. Bader Research group, *AIMPAC*, Hamilton, McMaster University, Canada.
[38] A. E. Reed, L. A. Curtiss, F. Weinhold, *Chem. Rev.* **1988**, *88*, 899.
[39] E. Uggerud, *Chem. Eur. J.* **2006**, *12*, 1127.
[40] S. G. Lias, H. M. Rosenstock, K. Deard, B. W. Steiner, J. T. Herron, J. H. Holmes, R. D. Levin, J. F. Liebman, S. A. Kafafi, J. E. Bartmess, E. F. Hunter, in *NIST Chemistry Webbook*, http://webbook.nist.-goc/chemistry, 2005.

Received: October 12, 2007
Published online: March 11, 2008

